Chemical Engineering Journal 498 (2024) 154898

Contents lists available at ScienceDirect

Chemical Engineering Journal

journal homepage: www.elsevier.com/locate/cej

Enhanced electrochemical cyclability of composite sodium metal anode with inorganic-rich solid electrolyte interphase

Changqun Cen [a,1], Xiaoxue Yang [a,1], Xiancheng Wang [b], Lin Fu [a,e,*], Yuanjian Li [b], Ke Lu [c], Liqing He [d,*], Yongming Sun [b,*]

[a] Provincial Guizhou Key Laboratory of Green Chemical and Clean Energy Technology, School of Chemistry and Chemical Engineering, Guizhou University, Guiyang 550025, China
[b] Wuhan National Laboratory for Optoelectronics, Huazhong University of Science and Technology, Wuhan 430074, China
[c] Institutes of Physical Science and Information Technology, School of Materials Science and Engineering, Key Laboratory of Structure and Functional Regulation of Hybrid Materials of Ministry of Education, Anhui University, Hefei 230601, China
[d] Hefei General Machinery Research Institute Co., Ltd, Hefei 230031, China
[e] International Academy of Optoelectronics at Zhaoqing, South China Normal University, Zhaoqing 526060, China

ARTICLE INFO

Keywords:
Sodium metal anode
Solid electrolyte interphase
Fast ion diffusion
Na/Na_3P composite foil
Electrochemical performance

ABSTRACT

The practical application of sodium (Na) metal anode in rechargeable batteries is impeded by inferior electrochemical properties and safety hazards arising from uneven Na plating/stripping behaviors. The Na-ion diffusion within the solid electrolyte interphase (SEI) plays a pivotal role in influencing these behaviors and the electrochemical performance of the Na metal anode. In this study, we leveraged the spontaneous reaction between red phosphorus (P) and metallic Na to fabricate a Na/Na_3P (NNP) composite foil using a straightforward folding and mechanical rolling method at room temperature. The *in-situ* formed Na_3P phase fosters the formation of an inorganic-rich SEI layer with high ionic conductivity, effectively enhancing the Na-ion diffusion kinetics and curbing the formation of Na dendrites. Moreover, the Na_3P present in the NNP composite can continually replenish the functional component and promptly repair the fracture of the SEI layer, thereby ensuring the stability of its structure and properties. Consequently, the NNP composite electrode significantly extends the Na plating/stripping cyclic lifespan compared to a bare Na anode. As a demonstration, the $Na_3V_2(PO_4)_3||$NNP full cell exhibits stable performance over 400 cycles with 96.7 % capacity retention at 5C. This work paves the way for designing stable SEI layers with fast ion diffusion capability for alkali metal anodes, and the findings are anticipated to propel the development of alkali metal batteries.

1. Introduction

Rechargeable lithium (Li)-based batteries have played a critical role in various energy storage applications, such as mobile electronic devices, electric vehicles, and large-scale energy storage [1,2]. However, the scarcity of Li resources coupled with the associated high cost curtails its further development, necessitating the exploration for viable Li substitutes [3,4]. Among the potential alternatives, rechargeable sodium (Na)-based batteries emerge as a prominent choice, given that metallic Na offers lower cost, abundant resources, and chemical properties akin to those of Li [5]. It is of paramount importance to acknowledge that the energy density of current Na-based batteries is less than 160 Wh kg^{-1}, underscoring the pressing need to augment the energy density for the advancement of rechargeable Na-based batteries [6]. Metallic Na, with its highest theoretical specific capacity (1165 mAh g^{-1}) and lowest reduction potential (-2.714 V vs standard hydrogen electrode) among the Na-based battery anodes, is deemed an ideal choice for high energy density Na-based batteries [7–9].

However, when metallic Na anode is coupled with the commonly used organic electrolyte, an organic-rich solid electrolyte interphase (SEI) layer is instantaneously formed owning to its high reactivity [10]. This organic-rich SEI layer, often characterized by its brittleness, fails to withstand the substantial volume change during repeated plating/stripping processes, thereby leading to its continuous cracking/

---

* Corresponding authors.
E-mail addresses: fulin.xr@foxmail.com (L. Fu), heli_limao@163.com (L. He), yongmingsun@hust.edu.cn (Y. Sun).
[1] These authors contributed equally to this work.

https://doi.org/10.1016/j.cej.2024.154898
Received 28 April 2024; Received in revised form 16 July 2024; Accepted 15 August 2024

reformation [11,12]. Also, the Na-ion diffusion in the organic-rich SEI is slow and uneven [13,14]. As a result, Na metal anode is subjected to uncontrollable Na dendrite growth, rapid formation of “dead Na” and compromised electrochemical stability [15]. Therefore, the construction of a more robust SEI layer, surpassing the conventional organic-rich one, is of paramount importance.

The integration of inorganic-rich components is perceived as beneficial for enhancing both the mechanical and electrochemical stability, and ionic conductivity of the SEI, consequently leading to the improvement of the electrochemical stability of the Na metal anode [16–18]. Upon integration with inorganic Na compounds, the SEI often exhibits enhanced ionic conductivity, thereby facilitating rapid Na-ion diffusion and improving electrochemical Na plating behaviour [8,19]. Furthermore, these inorganic compounds are typically characterized by a high interfacial energy and a substantial Young’s modulus [20,21]. These attributes are advantageous in promoting Na-ion diffusion along the SEI/Na interface and in mitigating the formation of Na dendrites. The utilization of electrolyte additives and the construction of an artificial interface layer with Na compounds on the Na metal anode surface can facilitate the formation of an inorganic-rich SEI [13,14,22]. For example, the Na-Sn alloying interface, achieved through an ion-exchange reaction, facilitated rapid Na-ion diffusion through the SEI layer [23], significantly contributing to the enhancement of electrochemical performances. Nonetheless, these strategies are susceptible to degradation or impairment during incessant cyclic operations, frequently resulting in an inadequate cyclic lifespan and restricted rate capacity [24]. Therefore, it is imperative to devise alternative strategies to achieve a stable and enduring SEI with high ionic conductivity. One promising approach could be the direct incorporation of an ionic conductivity composition throughout the entire electrode architecture [25]. Specifically, research has indicated that lithium phosphide (Li_3P), when used as an artificial SEI component, exhibits superior lithium-ion transport capabilities, thereby enhancing the electrochemical performance of the lithium metal anode [26,27]. Furthermore, red phosphorus (P) is a cost-effective and non-toxic alternative, and its reaction product with metallic Na, sodium phosphide (Na_3P), also exhibits high ionic conductivity, comparable to that of Li_3P [28,29]. The SEI with high ionic conductivity can ensure the rapid Na-ion transfer at electrode surface and inhibit the Na dendrite growth [30]. Yu and co-workers have demonstrated the efficacy of a Na_3P interface protective layer for the Na metal anode, which was constructed by repeatedly surface grinding Red P powder onto the Na metal surface [31]. Nonetheless, as the cycling process intensifies, the as-constructed protective layer begins to fracture. This leads to the formation of a new native SEI that differs in composition and structure from the initial one, thereby compromising its effectiveness in protecting against the Na metal electrode. Consequently, incorporating a functional component within the composite electrode to sustainably repair the fractures in the SEI layer presents an effective strategy for the advancement of Na metal anode technology (Fig. S1). On the other hand, the ion-conductive scaffolds have been verified to be effective in enabling uniform Na-ion flux, improving the Na-ion diffusion kinetics and suppressing the volume expansion, thus improving the cycle life of Na metal electrode [32,33].

Motivated by these insights, we construct a robust, ionically conductive SEI layer consisting of Na_3P through the construction of Na/Na_3P (NNP) composite electrode. The fabrication process, which involves repeated mechanical rolling of red P and metallic Na at room temperature, facilitates the production of ultrathin Na_3P and its uniform integration with metallic Na. Notably, the surficial Na_3P in the NNP composite electrode, which is accessible to the electrolyte, actively contributes to the formation of the SEI layer, thereby enabling fast Na-ion diffusion capability through the SEI layer and improvement of electrochemical behavior of metallic Na. Importantly, the Na_3P in the NNP composite can sustainably replenish the functional component and timely repair the fracture of the SEI, enabling the stability of its structure and property. As a result, the symmetric cell with the NNP composite electrode demonstrates a markedly reduced overpotential, significantly extended cyclic lifespan, and an extraordinary rate property when compared to the bare Na electrode. When paired with $Na_3V_2(PO_4)_3$ cathode to assemble full cell, the cell displays stable cycling with capacity retention of 96.7 % after 400 cycles at 5*C*, which is significantly better than the counterpart with a bare Na anode.

2. Experiment section

2.1. Synthesis of NNP composite foil

NNP composite foil was synthesized through the reaction between red P and an excess of metallic Na, facilitated by repeated folding and mechanical rolling operations. Na lumps, stored in mineral oil, were meticulously cleaned with a blade and subsequently rolled to form a Na foil. Thereafter, red P powders were uniformly coated on the Na foil surface. This was followed by repeated folding and mechanical rolling to ensure a complete reaction resulting in a uniform structure. All the aforementioned processes were conducted in an Ar-filled glovebox. Considering both specific capacity and cycling stability, a 9:1 mass ratio of metallic Na to red P was employed to fabricate the NNP composite foil, which served as the object of study.

2.2. Synthesis of $Na_3V_2(PO_4)_3$

$Na_3V_2(PO_4)_3$ powders were fabricated utilizing a sol–gel method [34,35]. Specifically, 0.09 g of V_2O_5 and 0.27 g of oxalic acid were dissolved in 30 ml of deionized water *via* magnetic stirring in oil bath at 75 °C. Subsequently, 0.27 g of $NH_4H_2PO_4$ and 0.14 g of Na_2CO_3 were introduced into the solution with continuous stirring and heating evaporation, resulting in a blue gel. The blue gel was dried at 100 °C overnight to yield a precursor. Finally, the precursor was thoroughly ground and preheated at 350 °C for 4 h followed by heated at 800 °C for 8 h in a 5 vol% H_2/Ar atmosphere to obtain $Na_3V_2(PO_4)_3$.

2.3. Material characterizations

The compositional and morphological characteristics of NNP composite foil were determined using X-ray diffraction (XRD) patterns (PANalytical B.V.) with Cu-Kα1 radiation (operating at a voltage of 40 kV and a current of 40 mA), Field emission scanning electron microscope (FE-SEM, GeminiSEM300) and X-ray photoelectron spectroscopy (XPS, AXIS-ULTRA DLD-600 W). For XRD measurements, the initial samples were positioned on a glass slide and encapsulated with Kapton tape in an Ar-filled glovebox. For the sake of original surface observation by SEM and XPS, the electrode samples were prepared by dissembling symmetric cells with pure Na or NNP composite electrodes. Then, they were put into an airtight transfer box and transferred to the SEM chamber. The transfer box can be easily opened by gravity inside the SEM, ensuring the preservation of good vacuum conditions prior to opening.

2.4. Electrochemical measurements

$Na_3V_2(PO_4)_3$ powders (80 wt%), polyvinylidene fluoride (PVDF, 10 wt%) and carbon black (10 wt%) were mixed in N-Methyl-2-pyrrolidone (NMP) to form a uniform slurry. The slurry was subsequently cast onto an Aluminum (Al) foil and dried at 60 °C for 6 h under vacuum conditions, resulting in the fabrication of the $Na_3V_2(PO_4)_3$ electrode. The mass loading of the $Na_3V_2(PO_4)_3$ cathode is about 5 mg cm^{-2} and corresponding areal capacity is about 0.55 mAh cm^{-2}. The specific capacity of full cells in our manuscript is calculated based on total mass of $Na_3V_2(PO_4)_3$, binder and conductive black. Coin-type cells (CR2032) were assembled in an Ar-filled glovebox. Glass fiber (Whatman GF/D) was employed as the separator and electrolyte composed of 1 M $NaClO_4$ in a 1:1 ratio of ethylene carbonate (EC)/diethyl carbonate (DEC), with 5 % fluoroethylene carbonate (FEC), was incorporated into each cell.

Electrochemical impedance spectroscopy (EIS) tests for different cycles were conducted on a Biologic VMP3 workstation, while temperature-varied tests were performed on Biologic SP-50, aided by a BE-TH thermostatic box. The frequency range for EIS tests spanned from 50 mHz to 1 MHz. Galvanostatic charge/discharge measurements were executed on a Neware battery test system. The NNP||NNP and Na||Na symmetric cells for Na plating/stripping cycles were tested at fixed current densities and fixed areal capacities. The $Na_3V_2(PO_4)_3$||NNP and $Na_3V_2(PO_4)_3$||Na full cells were initially activated at 0.5*C* (1*C*=110 mA g^{-1}) for 3 activation cycles, followed by constant charged/discharged at 5*C*, with the cut-off voltage ranging from 2.5 V to 4 V.

3. Results and discussion

An inorganic-rich SEI layer with fast Na-ion diffusion capability was realized *via* the fabrication of a Na-based composite foil, specifically composed of Na_3P known for its high ionic conductivity. As shown in Fig. S2, the Na_3P were introduced *via* repeated mechanical rolling/folding operations using red P powders and excess metallic Na as raw materials. This represents a viable strategy for the direct incorporation of Na_3P into the metallic Na electrode. During the fabrication, red P powders, as depicted in the XRD pattern and SEM image in Fig. S3 and Fig. S4, respectively, were initially coated onto the surface of a Na metal foil. Subsequently, repeated rolling and folding processes were employed to ensure the relatively uniform distribution of red P within the Na substrate, facilitating its sufficient reaction with Na at the P/Na interface. This process ultimately led to a complete transformation into Na_3P.The reaction can be described as “i.e., $P + (3 + x)\ Na \rightarrow Na_3P+x\ Na$”.

As shown in Fig. 1, the relatively uniformly distributed Na_3P particles on NNP composite electrode surface participate in the formation of SEI layer to regulate the electrochemical behavior of metallic Na and strengthen the mechanical properties of SEI layer. The Na_3P on the electrode surface accessible to electrolyte takes part in the SEI formation. The commendable ionic conductivity of Na_3P, approximately 0.12 mS cm^{-1}, can augment Na-ion diffusion through the SEI layer [31]. This enhancement facilitates the translocation of Na-ion along the anode surface, culminating in planar Na plating with a substantial particle size, oriented perpendicular to the SEI layer [36]. On the other hand, the presence of inorganic Na_3P particles improve the interface energy and Young’s modulus of the entire SEI layer, which can effectively suppress the formation of Na dendrites and maintain the stabilization of SEI layer [37,38]. Simultaneously, the existence of Na_3P within the bulk of NNP composite can perpetually mend the fractures in the SEI layer in a timely manner, thereby preserving the stability of its structure and properties. By contrast, the SEI formed on the surface of bare Na electrodes are fragile and cannot withstand the volume changes and dendrite growth during Na-ion plating/stripping, and will constantly breaking/reforming, ultimately forming a thick and uneven SEI. Furthermore, the simplicity of the material preparation process is advantageous for large-scale production in practical applications.

As anticipated, the electrochemical performance of the NNP composite electrode progressively improves with the incremental introduction of red P content. As highlighted in Fig. S5, the electrochemical performance improves as the red P content increases. Furthermore, as depicted in Fig. S6a, the overpotential of symmetric cells is categorized into three regions (I, II, and III) during the initial cycle. The nucleation overpotential of the NNP electrode with 15 wt% P is lower than that with 10 wt% P (Fig. S6a), which could result in more uniform Na plating behavior. However, its specific capacity is obviously inferior to the NNP electrode with 10 wt% P (754 vs. 795 mAh/g, Fig. 2a and S6b). In order to sustain the overall high electrochemical performance of the Na metal anode, a NNP composite electrode, introducing 10 wt% P, was chosen as the subject of our experiment. This capacity is more than double that of the commercial hard carbon anode [39], thereby indicating significant potential for application in high energy density batteries. The phase composition information of as-fabricated NNP composite foil is verified by the results of X-ray diffraction (XRD) measurement. As illustrated in Fig. 2b, the XRD pattern of the NNP composite foil, when compared to the bare Na foil, not only retains all diffraction peaks of metallic Na but also exhibits two additional diffraction peaks at approximately 35.97° and 36.96° (2θ), respectively. These peaks correspond to the (1 1 0) and (1 0 3) planes of Na_3P. The observed weak and broad characteristics confirm the smaller particle size of Na_3P. Beyond the diffraction peaks of Na and Na_3P, no other peaks are discernible in the XRD pattern of the NNP composite foil. This suggests that during the preparation processes,

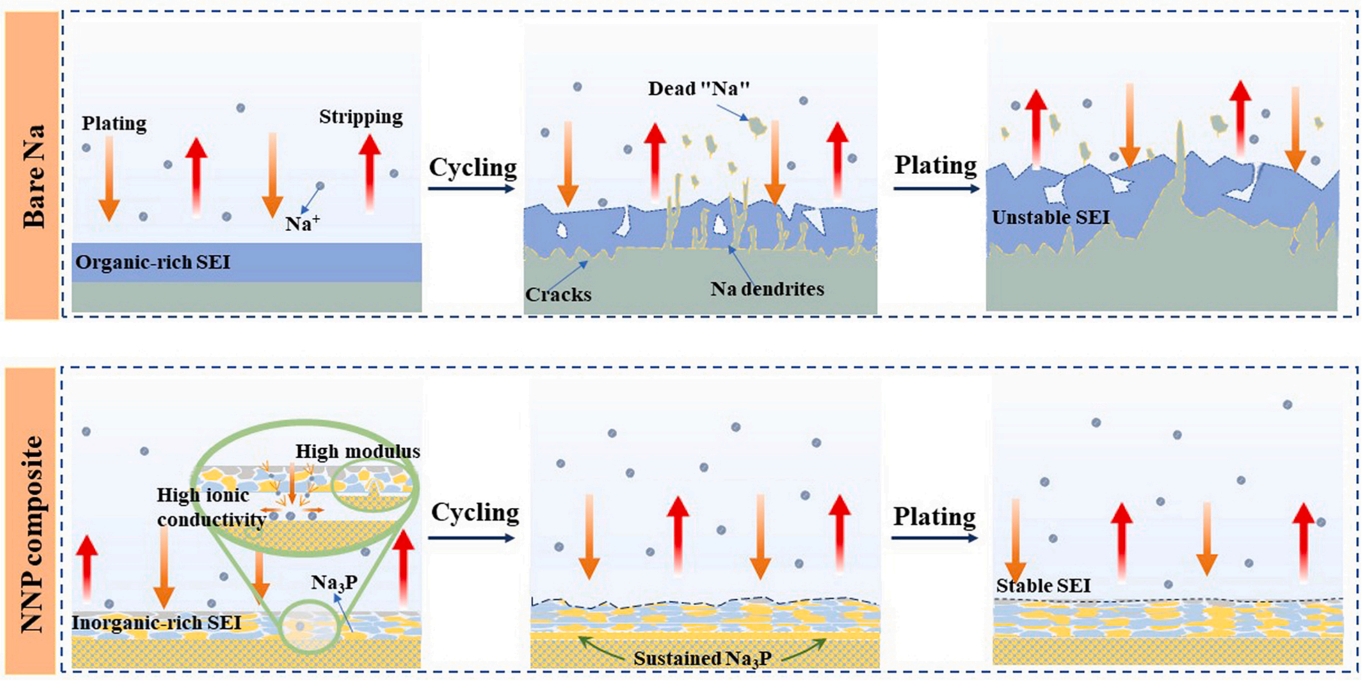

Fig. 1. Schematic of the effect of robust inorganic-rich SEI with ionic conductivity on stabilizing anode-electrolyte interface.

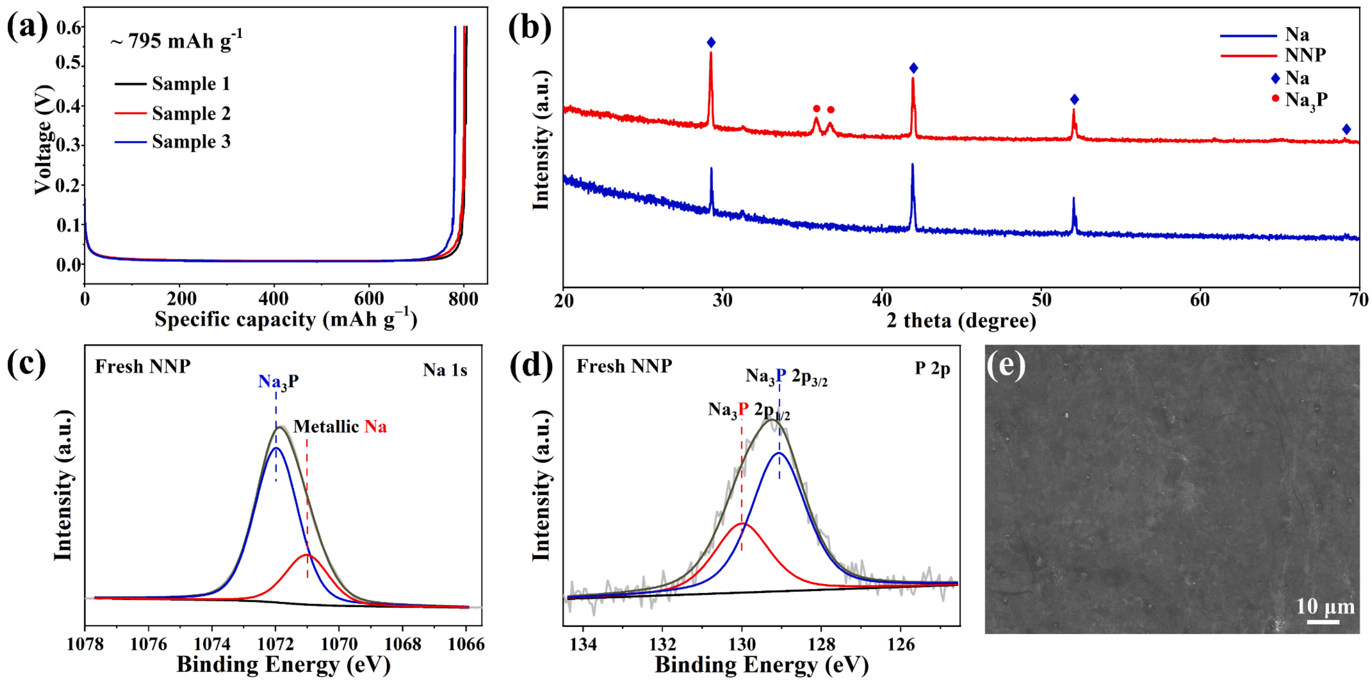

Fig. 2. (a) Complete Na stripping curve of the NNP composite electrode under the current density of 0.2 mA cm^{-2}. (b) XRD patterns of the Na and NNP composite foil. High-resolution (c) Na 1 s and (d) P 2p XPS spectra of NNP composite foil. (e) Top-view SEM image of the NNP composite foil.

the red powders have fully reacted with the metallic Na to form Na_3P. X-ray photoelectron spectroscope (XPS) is employed to further investigate the chemical composition of the NNP composite foil. The peaks in the high-resolution Na 1 s XPS spectrum (Fig. 2c) demonstrates two characteristic signals for metallic Na (1071.03 eV) and Na_3P (1072 eV) [40]. The P 2p core-level spectrum, as presented in Fig. 2d, exhibits two prominent peaks at 129.63 and 128.76 eV. These peaks are associated with the characteristic orbits of Na_3P 2p1/2 and 2p3/2, respectively [37,41]. The result confirms the co-existence of Na and Na_3P in the NNP composite foil. Scanning electron microscope (SEM) image (Fig. 2e) verifies that the surface of the NNP composite foil is smooth with compact structure, which is favorable for forming a stable interface and endowing uniform and fast Na-ion diffusion. As depicted in Fig. S7, which presents the digital images of both the bare Na and the NNP composite foil, the surface of the NNP composite foil appears smoother than that of the bare Na of equivalent thickness. This smoothness can be attributed to enhanced mechanical durability with the introduction of Na_3P. In contrast, the surface of the bare Na exhibits noticeable scratches. Significantly, the EDS mapping images, as illustrated in Fig. S8, reveal a relatively uniform distribution of Na and P within the

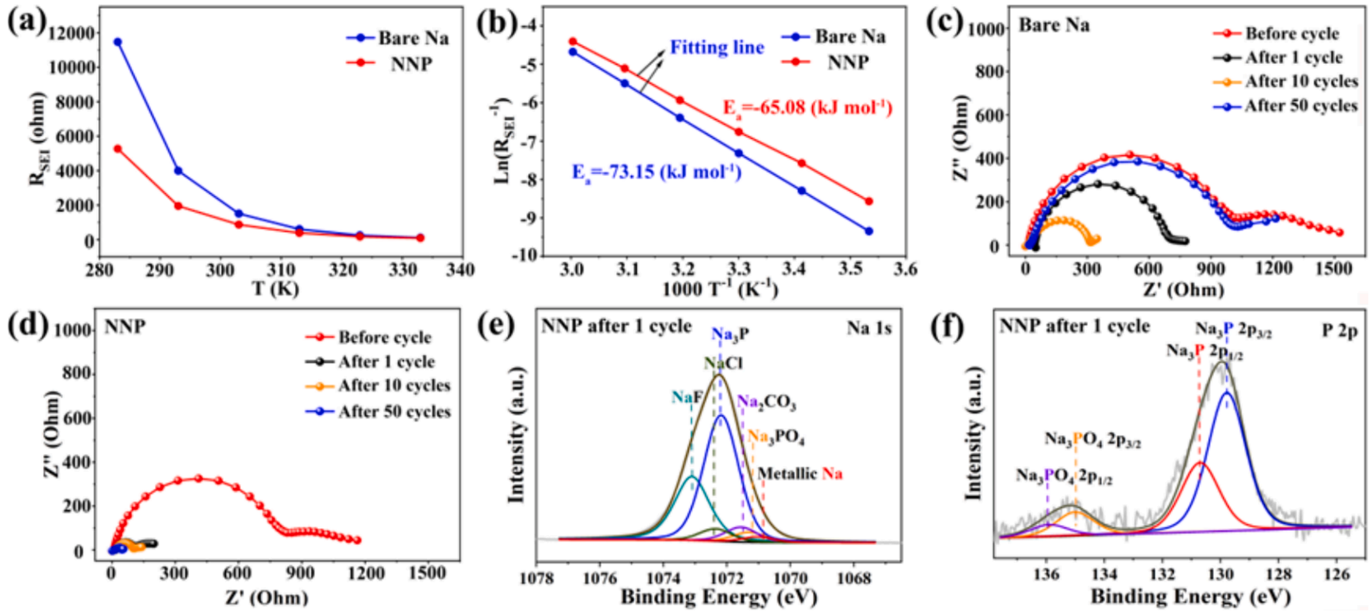

Fig. 3. (a) Interfacial impedances after fitting for NNP||NNP and Na||Na symmetric cells tested at different temperature and (b) linearly fitting of interfacial impedance and temperature according to the relationship in Arrhenius formula. Nyquist plots for (c) NNP||NNP and (d) Na||Na symmetric cells with different cycles under the current density of 1 mA cm^{-2} with a fixed capacity of 1 mAh cm^{-2}.High-resolution(e) Na 1 s and (f) P 2p XPS spectra of the NNP composite electrode after the initial cycle.

NNP composite foil. The cross-sectional SEM image of the NNP composite exhibits a dense structure, which can mitigate the side reaction between electrode and electrolyte, thereby improving the its electrochemical performance (Fig. S9). The corresponding EDS mapping images are consistent with the results of surface. This suggests that Na_3P is uniformly embedded within the Na matrix, a factor that is conducive to the formation of a homogeneous and robust SEI.

To further explore the SEI properties of the NNP composite electrode, the energy barrier associated with Na-ion diffusion through the SEI layer was examined, which were conducted *via* by employing an EIS test on both NNP||NNP and Na||Na symmetric cells under varying temperature gradients. As shown in Fig. 3a, the interface impedances of SEI layer (R_{SEI}) are obtained by fitting the Nyquist plots with the equivalent circuit (Fig. S10 and Fig. S11). Relationship between R_{SEI} and temperature (T) is described in Arrhenius formula, "i.e., $R_{SEI}^{-1} = A\exp(-E_a/RT)$ " [42]. By fitting ln (R_{SEI}^{-1}) with T^{-1} linearly energy barrier E_a for Na-ion diffusion through the SEI was obtained. As depicted in Fig. 3b, the value of E_a for the NNP composite electrode is significantly lower than that of the bare Na (−65.08 and − 73.15 KJ mol^{-1}, respectively), suggesting that Na-ion diffusion through the SEI of the NNP composite electrode is more facile. The Tafel plots, as illustrated in Fig. S12 corroborate this observation, the exchange current density in the NNP composite electrode has increased from 0.143 to 0.202 mA cm^{-2}, indicative of enhanced Na-ion diffusion kinetics. The energy barrier analysis reveals that the formation of an Na_3P-containing SEI, exhibits accelerated Na-ion diffusion properties, which are advantageous for enhancing battery performance.

To further explore the positive effect Na_3P for the improved SEI properties, EIS test was carried out for NNP||NNP and Na||Na symmetric cells with different cycles under the current density of 1 mA cm^{-2} with a fixed capacity of 1 mAh cm^{-2}. As shown in Fig. 3c and d, the interfacial impedance of the NNP composite electrode before cycling is significantly lower than the bare Na electrode (~810 and 1020 O, respectively), demonstrating that the Na_3P can effectively suppress side reactions between electrode and electrolyte and promote Na-ion diffusion through the SEI layer [31]. In addition, the interfacial impedance of the bare Na electrode decreased to ~ 700 O after 1 cycle and rapidly decreased to ~ 310 O after 10 cycles, which is attributed to the breaking of native oxide layer and increasing surface area caused by dendrites growth and proliferation [43,44]'. As the Na dendrites proliferate and the SEI undergoes continuous cycles of rupture and repair, inactive Na accumulates progressively, leading to the persistent consumption of the electrode [45]. Consequently, the interfacial impedance of the bare Na escalated to ~ 1000 O after 50 cycles. In contrast, the interfacial impedance of the NNP composite electrode significantly reduced to ~ 100 O after a single cycle, subsequently maintaining a low and stable interfacial impedance (~45 O following 50 cycles). These findings underscore that the formation of an inorganic-rich SEI, resulting from the involvement of Na_3P, enhances Na-ion diffusion and sustains interface stability. Furthermore, utilizing voltage response to a direct current of 5 mA (Fig. S13), the electronic conductivity of the bare Na and NNP composite foil was calculated using Equation (S1) [46]. The calculated electronic conductivity of the NNP composite electrode was ≈ 4.2 x 10^{-4} S m^{-1}, which is lower than that of the bare Na (≈ 1.59 x 10^{-3} S m^{-1}). This outcome facilitates the swift transfer of electrons on the surface of the interfacial NNP composite electrode [47,48].

To investigate the composition of the SEI, XPS analysis was conducted on the NNP composite after the initial cycle, following a 10-minute Ar-ion etching process. As depicted in Fig. 3e and f, the peak at 1072.16 eV in the high-resolution Na 1 s spectrum, along with the peaks at 129.78 and 130.7 eV in the high-resolution P 2p spectrum, confirm the presence of Na_3P [49,50]. The Na 1 s core level region also exhibits three characteristic peaks at 1071.54, 1072.35 and 1073.09 eV, which can be ascribed the signals of Na_2CO_3, NaCl and NaF [51,52], respectively. The presence of these species can be further confirmed by the high-resolution spectra of F 1 s, C 1 s, Cl 2p and O 1 s, as depicted in Fig. S14, respectively. Moreover, distinct from the fresh NNP composite foil, two new peaks are observed in the XPS P 2p spectrum at 135.01 eV and 135.9 eV, respectively. These peaks can be ascribed to the 2p3/2 and 2p1/2 orbits of Na_3PO_4 [53]. The corresponding characteristic peaks are discernible in the Na 1 s spectrum at 1071.29 eV [54]. Na_3PO_4 and NaF serve as advantageous interfacial stabilizer for Na metal anode [55,56], facilitating the modulation of the plating/stripping behavior of metallic Na. It is imperative to underscore that Na_3P originates from the electrode composition, whereas Na_3PO_4, Na_2CO_3, and NaF are likely to be derived from the decomposition of the electrolyte composite on the surface of the NNP composite electrode [11,57]. Inorganic rich components of the SEI, including Na_3P, Na_3PO_4, Na_2CO_3 and NaF, form a stable Na-ion diffusion layer, thereby promoting Na-ion diffusion in it. The XPS spectra of NNP electrode after 10 cycles (Fig. S15) are highly consistent with the results of NNP after 1 cycle, which demonstrates that Na3P can help to stabilize the interface of electrode, enabling the stability of its structure and property.

Na plating/stripping behaviors were scrutinized using SEM to observe the post-cycling electrode structure. Large and deep cavities are presented in the surface of the bare Na electrode after initial Na stripping under the current density of 1 mA cm^{-2} with a fixed capacity of 1 mA h cm^{-2} (Fig. 4a). As a contrast, the NNP composite electrode displayed a relatively smooth surface under the same test condition (Fig. 4**d**), indicating that the inorganic-rich SEI for NNP electrode can adjust the Na-ion flux and enable uniform Na stripping. In the case of Na plating, the bare Na electrode displayed mossy and dendritic structures (as depicted in Fig. 4b). These structures are associated with uncontrolled dendrite growth, leading to the sequential consumption of active Na and electrolyte. Conversely, for the NNP composite electrode, a phenomenon of grain coarsening is observed during NNP plating (as shown in Fig. 4e). This results in the formation of smooth and granular Na depositions, with sizes exceeding 3 μm. The improved Na plating/stripping behaviors for the NNP composite electrode can be attributed to the fast and uniform Na-ion diffusion through the SEI, which are favorable for cycling stability and safety of batteries. The digital photos of bare Na and NNP composite electrodes distributed in DMC after 50 cycles and the schematic diagram of Na plating/stripping during those processes are shown in Fig. 4c and f. It is noteworthy that the DMC solution of the cycled NNP composite electrode appears cleaner than that of the cycled bare Na electrode. In the DMC solution of the cycled bare Na electrode, conspicuous suspended impurity solids are observed, which may be the inactive Na produced during the cycling. As depicted in the schematic of the Na plating/stripping processes, the Na ions of the NNP composite electrode can be uniformly deposited on the electrode surface, thereby avoiding the formation of disordered dendrites/mossy structure, a characteristic feature of the bare Na electrode. These results indicate that the existence of Na_3P in the NNP composite electrode is beneficial to the formation of uniform and stable interphase layer, increasing the Na-ion diffusion rate and promoting the uniform Na metal deposition. Moreover, the composite structure of the NNP significantly contributes to the enhanced structural stability of the electrode. The Na_3P phase, relatively uniformly distributed within the metallic Na matrix, serves as an effective buffer against volume changes during the Na stripping/plating processes. This diminished overall volume fluctuation could potentially alleviate the stress and strains imposed on the SEI, thereby further bolstering the stability of the SEI. This, in turn, enhances the electrochemical cycling stability.

To evaluate the cycling stability of the NNP composite foil, NNP||NNP and Na||Na symmetric cells were assembled and galvanostatic Na plating/stripping cycling tests were performed. The average Coulombic efficiency (CE) was used to evaluate reversibility of NNP anode according to the previous reported method [58]. The average CE of NNP electrode is as high as 95.38 % for Na plating/stripping cycles under a current density of 1 mA cm^{-2} with a fixed capacity of 1 mAh cm^{-2}, while bare Na electrode only reaches 77.2 % (Fig. S16). These results indicated that the presence of Na3P contributes to the formation of stable SEI, which inhibits the side reaction between Na and electrolyte, thus

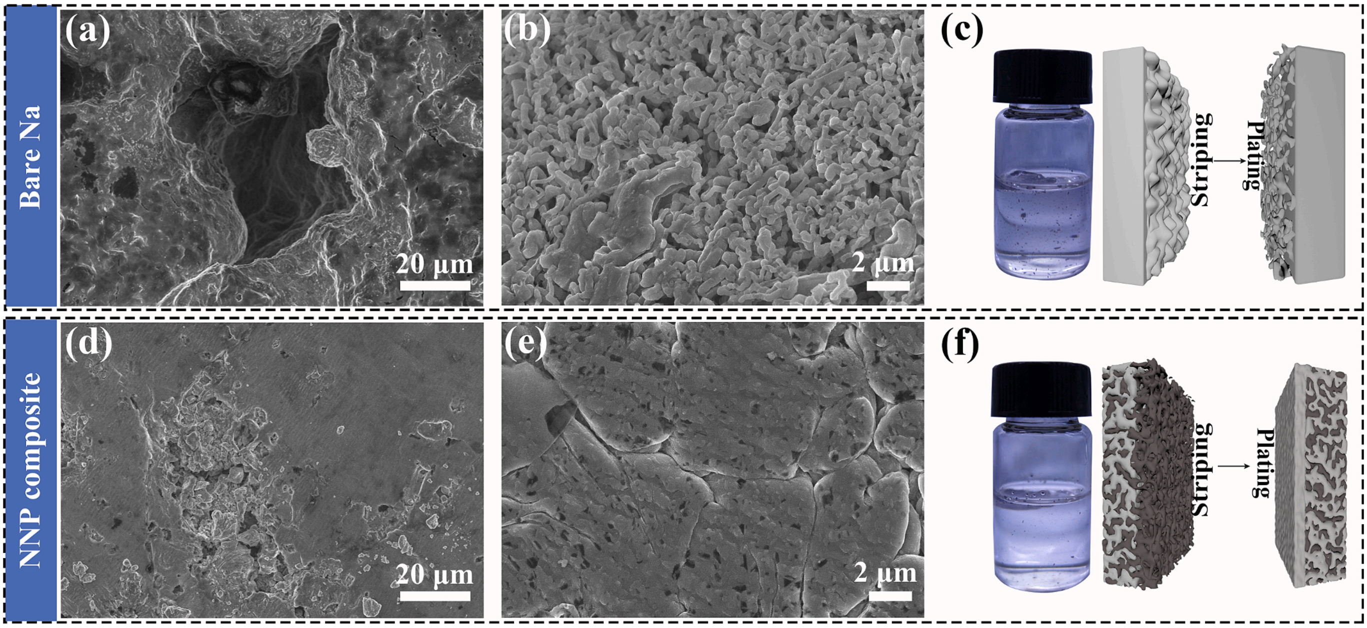

Fig. 4. The SEM images of the bare Na electrode after Na (a) stripping and (b) plating at a current density of 1 mA cm^{-2} with a fixed capacity of 1 mAh cm^{-2}. (c) Digital photos of the bare Na electrode resting in DMC after 50 cycles and the schematic of the plating/stripping processes. The SEM images of the NNP composite electrode after Na (d) stripping and (e) plating at a current density of 1 mA cm^{-2} with a fixed capacity of 1 mAh cm^{-2}. (f) Digital photos of NNP electrode resting in DMC solution after 50 cycles and the schematic of the plating/stripping processes.

reducing the consumption of active Na. Supported by the fast Na-ion diffusion capability of the SEI, the symmetric cell with NNP composite electrode showed flat and smooth voltage profiles with very low overpotential, as well as greatly extended cyclic lifespan over 500 h under a current density of 1 mA cm^{-2} with a fixed capacity of 1 mAh cm^{-2} (Fig. 5a). The expanded voltage profiles demonstrate that the voltage profiles of the NNP composite electrode, even after 200 cycles, remain consistent and exhibit negligible overpotential increase compared to the 20th cycle (Fig. 5b). This suggests the persistent existence of a stable, inorganic-rich interface layer. In stark contrast, the symmetric cell with bare Na displays pronounced voltage fluctuation and high overpotential (ranging from ~ 50 mV to ~ 150 mV). This is attributable to aforementioned poor Na-ion diffusion ability through the SEI and the uneven Na plating/stripping behavior during the cycling processes. Furthermore, solid evidence has unequivocally demonstrated that the side reactions of the Na anode are intimately linked to the decay in electrochemical performance [59–61]. The presence of Na3P could reduce the chemical reactivity of NNP composite electrode to organic electrolyte, thus prolonging its cycling life. The overpotential of bare Na abruptly decreases after cycling for 80 h, a clear indication of cell short circuit, likely due to dendrite puncture [62]. The ion transport efficiency of SEI layer plays a pivotal role in ensuring stable Na plating/stripping cycles under high current density.

Fig. 5c juxtaposes the voltage profiles of the NNP composite and bare Na electrodes under the current densities ranging from 0.5 to 5 mA cm^{-2} and back to 0.5 mA cm^{-2}, with a fixed capacity of 1 mAh cm^{-2}. The NNP composite electrode maintains stable voltage profiles and low overpotential even at 5 mA cm^{-2} (Fig. 5d). Also, a negligible change in overpotential is observed between the first and the last 10 cycles under same current density. This suggests that the NNP composite electrode exhibits excellent rate capability, benefiting from fast Na-ion diffusion through SEI. In contrast, the bare Na not only exhibits pronounced voltage fluctuation but also experiences a short circuit when the current density reverts to 0.5 mA cm^{-2} after enduring high current conditions (3 mA cm^{-2} and 5 mA cm^{-2}). This indicates its inferior rate property, which can be attributed to the unstable interface with low Na-ion diffusion capability. More specifically, when cycled at a current density of 1 mA cm^{-2} with a fixed of 3 mAh cm^{-2} (Fig. S17), the symmetric cell with the NNP composite electrode exhibits stable voltage profiles even for 500 h, while the bare Na electrode only cycles about 80 h. The superior electrochemical performance of the NNP composite electrode under the high capacity supports that Na_3P in the NNP composite participates in the formation of SEI during the cycling, which directly improve ionic conductivity and mechanical property of SEI. As per the 10th cycle galvanostatic profile for NNP||NNP and Na||Na symmetric cells at 1 mA cm^{-2} and 1 mAh cm^{-2} (Fig. S18), the Na||Na symmetric cell exhibits two distinct voltage plateaus, corresponding to a capacity retention of approximately 92.3 % and a capacity loss of 7.6 %, respectively. This suggests that the Na-ion reacts with the electrolyte to form inactive Na during the cycle. As a contrast, the NNP||NNP symmetric cell displays a single, extended voltage plateau, confirming that the involvement of Na_3P effectively stabilizes the SEI and prevents the side reaction of the composite anode with electrolyte [63].

Full cell with $Na_3V_2(PO_4)_3$ cathode were assembled to investigate the practicability of the NNP composite foil. As depicted in Fig. S19, nearly equivalent specific capacities and identical charge/discharge profiles are observed in both full cells at the initial 3 cycles, demonstrating stable electrochemical behavior of the NNP composite foil electrode. In addition, the long-term stability of Na_3P-containing electrode is demonstrated by the nearly equivalent specific capacities charge/discharge profiles after multiple cycles as shown in Fig. S20. Beneficial from the superior cycling stability of $Na_3V_2(PO_4)_3$, the $Na_3V_2(PO_4)_3$||Na cell exhibits stable cycling up to ~ 300 cycles, followed by a rapid specific capacity fading at 5*C* (1*C*=110 mA g^{-1}). In the case of employing NNP composite anode (Fig. 5e), the full cell sustains stable cycling for 400 cycles and maintains a high-capacity retention of 96.7 %. This can be attributed to the Na_3P in the NNP composite providing functional components for SEI repair, thereby maintaining the structural stability of SEI. These results underscore the significant role of Na_3P from the NNP composite in prolonging the cycle life of batteries. It's also worth noting that NNP composite electrode has superior high-rate charge/discharge capacity in comparison with bare Na electrode (Fig. 5f). The capacity difference gradually increases with the increase of current density. When the current density increased to 30*C*, the specific capacity of $Na_3V_2(PO_4)_3$||NNP full cell is still as high as 62.7 mAh g^{-1}, while the $Na_3V_2(PO_4)_3$||Na is closed to zero. Such results indicate that Na_3P with

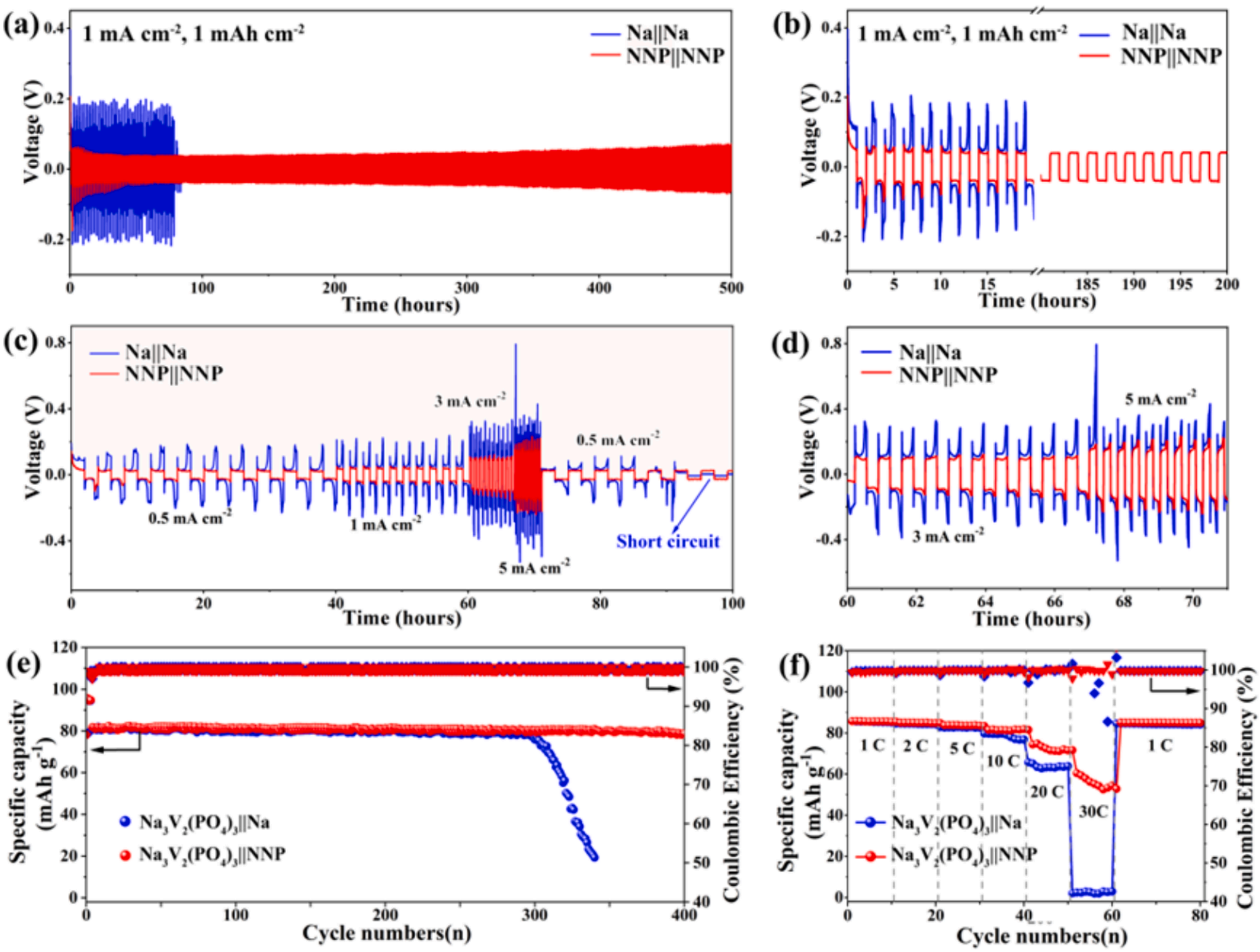

Fig. 5. (a) Voltage-time profiles of NNP||NNP and Na||Na symmetric cells at current density of 1 mA cm^{-2} with a fixed capacity of 1 mAh cm^{-2} and (b) the corresponding selected profiles. (c) Voltage-time profiles for cycling with fixed capacity of 1 mAh cm^{-2} at different current densities of 0.5, 1, 3, 5, and back to 0.5 mA cm^{-2} and (d) the corresponding selected profiles. (e) Cycling performance of $Na_3V_2(PO_4)_3$||Na and $Na_3V_2(PO_4)_3$||NNP full cells at the current density of 5*C* (1*C*=110 mA g^{-1}). (f) Rate performances of $Na_3V_2(PO_4)_3$||Na and $Na_3V_2(PO_4)_3$||NNP full cells at the current density from 1 to 30*C*.

high ionic conductivity can promote the Na-ion diffusion and reduces the charge transfer impedance.

4. Conclusion

In conclusion, we have constructed an inorganic-rich SEI with rapid ion diffusion capability, achieved through use of the NNP composite foil, within which Na_3P is relatively uniformly distributed. The NNP composite foil was fabricated through repeated mechanical rolling and folding operations at room temperature, utilizing red P powders and excess metallic Na as raw materials. These repeated processes facilitate the warm reaction between red P and Na at the P/Na interface, ultimately resulting in the formation of ultrafine Na_3P particles relatively uniformly distributed throughout the entire Na metal matrix. Na_3P contributes to the formation of the SEI layer, together with other inorganic species, thereby enhancing both the ionic conductivity and mechanical strength of the SEI layer. Consequently, the electrochemical performance of the NNP composite electrode is improved, exhibiting reduced interface impedance, lower energy barrier of Na-ion diffusion through SEI, dendrite-free Na plating. and lower overpotential compared to the bare Na electrode. Moreover, the existence of Na_3P in NNP composite can continuously replenish the functional components to timely repair any fractures of the SEI, thereby maintaining its structure and properties stable. The NNP||NNP symmetric cell demonstrates stable electrochemical cycling properties, which are significantly superior to those of the Na||Na symmetric cell. When paired with a $Na_3V_2(PO_4)_3$ cathode, the NNP composite foil exhibits exceptional cycling stability and a high-capacity retention of 96.7 % at 5C after 400 cycles. This straightforward and efficient strategy could potentially be extended to other functional SEI layers of alkali metal anodes to enhance their electrochemical performance.

CRediT authorship contribution statement

Changqun Cen: Investigation, Data curation. **Xiaoxue Yang:** Investigation. **Xiancheng Wang:** Methodology. **Lin Fu:** Writing – original draft, Supervision, Funding acquisition. **Yuanjian Li:** Investigation. **Ke Lu:** Investigation. **Liqing He:** Investigation, Funding acquisition. **Yongming Sun:** Writing – review & editing, Funding acquisition, Conceptualization.

Declaration of competing interest

The authors declare that they have no known competing financial interests or personal relationships that could have appeared to influence the work reported in this paper.

Data availability

Data will be made available on request.

Acknowledgements

The authors would like to thank the financial support by National Natural Science Foundation of China (No. 52272207; 22209031; 52101249), Guizhou Provincial Basic Research Program (Natural Science) (No. QKHJC-ZK [2023] YB046), and Natural Science Special Foundation of Guizhou University (No. X2022122 Special Post B). The authors would like to thank the Analytical and Testing Center of the Huazhong University of Science and Technology and Wuhan National Laboratory for Optoelectronics of Huazhong University of Science and Technology for providing the facilities to conduct the characterization.

Appendix A. Supplementary data

Supplementary data to this article can be found online at https://doi.org/10.1016/j.cej.2024.154898.

References

[1] A. Manthiram, An outlook on lithium ion battery technology, ACS Cent. Sci. 3 (2017) 1063–1069, https://doi.org/10.1021/acscentsci.7b00288.

[2] A.K. Stephan, The age of Li-ion batteries, Joule 3 (2019) 2583–2584, https://doi.org/10.1016/j.joule.2019.11.004.

[3] F. Duffner, N. Kronemeyer, J. Tübke, J. Leker, M. Winter, R. Schmuch, Post-lithium-ion battery cell production and its compatibility with lithium-ion cell production infrastructure, Nat. Energy 6 (2021) 123–134, https://doi.org/10.1038/s41560-020-00748-8.

[4] C. Vaalma, D. Buchholz, M. Weil, S. Passerini, A cost and resource analysis of sodium-ion batteries, Nat. Rev. Mater. 3 (2018) 18013, https://doi.org/10.1038/natrevmats.2018.13.

[5] W. Zhang, F. Zhang, F. Ming, H.N. Alshareef, Sodium-ion battery anodes: status and future trends, EnergyChem 1 (2019) 100012, https://doi.org/10.1016/j.enchem.2019.100012.

[6] Y. Liao, L. Yuan, Y. Han, C. Liang, Z. Li, Z. Li, W. Luo, D. Wang, Y. Huang, Pentafluoro(phenoxy)cyclotriphosphazene stabilizes electrode/electrolyte interfaces for sodium-ion pouch cells of 145 Wh Kg^{-1}, Adv. Mater. 36 (2024) 2312287, https://doi.org/10.1002/adma.202312287.

[7] C. Delmas, Sodium and sodium-ion batteries: 50 years of research, Adv. Energy Mater. 8 (2018) 1703137, https://doi.org/10.1002/aenm.201703137.

[8] X. Xia, S. Xu, F. Tang, Y. Yao, L. Wang, L. Liu, S. He, Y. Yang, W. Sun, C. Xu, Y. Feng, H. Pan, X. Rui, Y. Yu, A multifunctional interphase layer enabling superior sodium-metal batteries under ambient temperature and −40 °C, Adv. Mater. 35 (2023) 2209511, https://doi.org/10.1002/adma.202209511.

[9] J.Y. Hwang, S.T. Myung, Y.K. Sun, Sodium-ion batteries: present and future, Chem. Soc. Rev. 46 (2017) 3529–3614, https://doi.org/10.1039/C6CS00776G.

[10] Y. Xiang, G. Zheng, Z. Liang, Y. Jin, X. Liu, S. Chen, K. Zhou, J. Zhu, M. Lin, H. He, J. Wan, S. Yu, G. Zhong, R. Fu, Y. Li, Y. Yang, Visualizing the growth process of sodium microstructures in sodium batteries by in-situ 23Na MRI and NMR spectroscopy, Nat. Nanotechnol. 15 (2020) 883–890, https://doi.org/10.1038/s41565-020-0749-7.

[11] Y. Ji, J. Qiu, W. Zhao, T. Liu, Z. Dong, K. Yang, G. Zheng, G. Qian, M. Yang, Q. Chen, K. Amine, F. Pan, L. Yang, In situ probing the origin of interfacial instability of Na metal anode, Chem 9 (2023) 2943–2955, https://doi.org/10.1016/j.chempr.2023.06.002.

[12] T. Liu, X. Yang, J. Nai, Y. Wang, Y. Liu, C. Liu, X. Tao, Recent development of Na metal anodes: interphase engineering chemistries determine the electrochemical performance, Chem. Eng. J. 409 (2021) 127943, https://doi.org/10.1016/j.cej.2020.127943.

[13] R. Damircheli, B. Hoang, V. Castagna Ferrari, C.F. Lin, Fluorinated artificial solid-electrolyte-interphase layer for long-life sodium metal batteries, ACS Appl, Mater. Interfaces 15 (2023) 54915–54922, https://doi.org/10.1021/acsami.3c12351.

[14] S. Wan, K. Song, J. Chen, S. Zhao, W. Ma, W. Chen, S. Chen, Reductive competition effect-derived solid electrolyte interphase with evenly scattered inorganics enabling ultrahigh rate and long-life span sodium metal batteries, J. Am. Chem. Soc. 145 (2023) 21661–21671, https://doi.org/10.1021/jacs.3c08224.

[15] Q. Chen, B. Liu, L. Zhang, Q. Xie, Y. Zhang, J. Lin, B. Qu, L. Wang, B. Sa, D. Peng, Sodiophilic Zn/SnO_2 porous scaffold to stabilize sodium deposition for sodium metal batteries, Chem. Eng. J. 404 (2021) 126469, https://doi.org/10.1016/j.cej.2020.126469.

[16] Y. Yu, H. Koh, Z. Zhang, Z. Yang, A.N. Alexandrova, M. Agarwal, E.A. Stach, J. Xie, Kinetic pathways of fast lithium transport in solid electrolyte interphases with discrete inorganic components, Energy Environ. Sci. 16 (2023) 5904–5915, https://doi.org/10.1039/d3ee02048g.

[17] Y. Jin, P.M.L. Le, P. Gao, Y. Xu, B. Xiao, M.H. Engelhard, X. Cao, T.D. Vo, J. Hu, L. Zhong, B.E. Matthews, R. Yi, C. Wang, X. Li, J. Liu, J.-G. Zhang, Low-solvation electrolytes for high-voltage sodium-ion batteries, Nat. Energy 7 (2022) 718–725, https://doi.org/10.1038/s41560-022-01055-0.

[18] M. Liu, F. Wu, Y. Gong, Y. Li, Y. Li, X. Feng, Q. Li, C. Wu, Y. Bai, Interfacial-catalysis-enabled layered and inorganic-rich SEI on hard carbon anodes in ester electrolytes for sodium-ion batteries, Adv. Mater. 35 (2023) 2300002, https://doi.org/10.1002/adma.202300002.

[19] W. Liu, X. Chen, C. Zhang, H. Xu, X. Sun, Y. Zheng, Y. Yu, S. Li, Y. Huang, J. Li, Gassing in Sn-anode sodium-ion batteries and its remedy by metallurgically prealloying Na, ACS Appl. Mater. Interfaces 11 (2019) 23207–23212, https://doi.org/10.1021/acsami.9b05005.

[20] Y. Jiang, Y. Yang, F. Ling, G. Lu, F. Huang, X. Tao, S. Wu, X. Cheng, F. Liu, D. Li, H. Yang, Y. Yao, P. Shi, Q. Chen, X. Rui, Y. Yu, Artificial heterogeneous interphase layer with boosted ion affinity and diffusion for Na/K-Metal batteries, Adv. Mater. 34 (2022) 2109439, https://doi.org/10.1002/adma.202109439.

[21] X. Xia, Y. Yang, K. Chen, S. Xu, F. Tang, L. Liu, C. Xu, X. Rui, Enhancing interfacial strength and wettability for wide-temperature sodium metal batteries, Small 19 (2023) 2300907, https://doi.org/10.1002/smll.202300907.

[22] J. Zhou, Y. Wang, J. Wang, Y. Liu, Y. Li, L. Cheng, Y. Ding, S. Dong, Q. Zhu, M. Tang, Y. Wang, Y. Bi, R. Sun, Z. Wang, H. Wang, Low-temperature and high-rate sodium metal batteries enabled by electrolyte chemistry, Energy Stor. Mater. 50 (2022) 47–54, https://doi.org/10.1016/j.ensm.2022.05.005.

[23] Z. Tu, S. Choudhury, M.J. Zachman, S. Wei, K. Zhang, L.F. Kourkoutis, L.A. Archer, Fast ion transport at solid-solid interfaces in hybrid battery anodes, Nat. Energy 3 (2018) 310–316, https://doi.org/10.1038/s41560-018-0096-1.

[24] Y. Gao, Z. Yan, J.L. Gray, X. He, D. Wang, T. Chen, Q. Huang, Y.C. Li, H. Wang, S. H. Kim, T.E. Mallouk, D. Wang, Polymer-inorganic solid-electrolyte interphase for stable lithium metal batteries under lean electrolyte conditions, Nat. Mater. 18 (2019) 384–389, https://doi.org/10.1038/s41563-019-0305-8.

[25] S. Zhang, Z. Yin, Z. Wu, D. Luo, Y. Hu, J. You, B. Zhang, K. Li, J. Yan, X. Yang, X. Zhou, S. Zanna, P. Marcus, F. Pan, J. Światowska, S. Sun, Z. Chen, J. Li, Achievement of high-cyclability and high-voltage Li-metal batteries by heterogeneous SEI film with internal ionic conductivity/external electronic insulativity hybrid structure, Energy Stor. Mater. 40 (2021) 337–346, https://doi.org/10.1016/j.ensm.2021.05.029.

[26] L. Fu, X. Wang, B. Zhang, Z. Chen, Y. Li, Y. Sun, A Li_3P nanoparticle dispersion strengthened ultrathin Li metal electrode for high energy density rechargeable batteries, Nano Res. 17 (2024) 4031–4038, https://doi.org/10.1007/s12274-023-6275-9.

[27] G. Nazri, Preparation, structure and ionic conductivity of lithium phosphide, Solid State Ion. 34 (1989) 97–102, https://doi.org/10.1016/0167-2738(89)90438-4.

[28] Q. Xu, J. Sun, F. Yue, J. Li, G. Li, S. Xin, Y. Yin, Y. Guo, Stable sodium storage of red phosphorus anode enabled by a dual-protection strategy, ACS Appl. Mater. Interfaces 10 (2018) 30479–30486, https://doi.org/10.1021/acsami.8b12571.

[29] X. Yu, G. Giorgi, H. Ushiyama, K. Yamashita, First-principles study of fast Na diffusion in Na_3P, Chem. Phys. Lett. 612 (2014) 129–133, https://doi.org/10.1016/j.cplett.2014.08.010.

[30] X. Lu, H. Zhao, Y. Qin, E. Matios, J. Luo, R. Chen, H. Nan, B. Wen, Y. Zhang, Y. Li, Q. He, X. Deng, J. Lin, K. Zhang, H. Wang, K. Xi, Y. Su, X. Hu, S. Ding, W. Li, Building fast ion-conducting pathways on 3D metallic scaffolds for high-performance sodium metal anodes, ACS Nano 17 (2023) 10665–10676, https://doi.org/10.1021/acsnano.3c01759.

[31] P. Shi, S. Zhang, G. Lu, L. Wang, Y. Jiang, F. Liu, Y. Yao, H. Yang, M. Ma, S. Ye, X. Tao, Y. Feng, X. Wu, X. Rui, Y. Yu, Red phosphorous-derived protective layers with high ionic conductivity and mechanical strength on dendrite-free sodium and potassium metal anodes, Adv. Energy Mater. 11 (2020) 2003381, https://doi.org/10.1002/aenm.202003381.

[32] X. Lu, X. Zhao, S. Ding, X. Hu, 3D mixed ion/electron-conducting scaffolds for stable sodium metal anodes, Nanoscale 16 (2024) 3379–3392, https://doi.org/10.1039/d3nr05814j.

[33] X. Lu, R. Chen, S. Shen, Y. Li, H. Zhao, H. Wang, T. Wu, Y. Su, J. Luo, X. Hu, S. Ding, W. Li, Spatially confined in situ formed sodiophilic-conductive network for high-performance sodium metal batteries, Nano Lett. 24 (2024) 5490–5497, https://doi.org/10.1021/acs.nanolett.4c00562.

[34] F. Li, Y.-E. Zhu, J. Sheng, L. Yang, Y. Zhang, Z. Zhou, GO-induced preparation of flake-shaped $Na_3V_2(PO_4)_3$@rGO as high-rate and long-life cathodes for sodium-ion batteries, J. Mater. Chem. A 5 (2017) 25276–25281, https://doi.org/10.1039/c7ta07943e.

[35] W. Duan, Z. Zhu, H. Li, Z. Hu, K. Zhang, F. Cheng, J. Chen, $Na_3V_2(PO_4)_3$@C core-shell nanocomposites for rechargeable sodium-ion batteries, J. Mater. Chem. A 2 (2014) 8668–8675, https://doi.org/10.1039/c4ta00106k.

[36] K. Lin, X. Xu, X. Qin, J. Wu, Q. Liu, Z. Tang, S. He, Y. Ye, F. Kang, B. Li, In situ constructed ionic-electronic dual-conducting scaffold with reinforced interface for high-performance sodium metal anodes, Small 17 (2021) 2104021, https://doi.org/10.1002/smll.202104021.

[37] Z. Luo, S. Tao, Y. Tian, L. Xu, Y. Wang, X. Cao, Y. Wang, W. Deng, G. Zou, H. Liu, H. Hou, X. Ji, Robust a artificial interlayer for columnar sodium metal anode, Nano Energy 97 (2022) 107203, https://doi.org/10.1016/j.nanoen.2022.107203.

[38] X. Zhu, Y. Wang, W. Wang, K. Wu, M. Zhu, G. Wang, G. Xu, M. Wu, H. Liu, S. Dou, C. Wu, Stable sodium metal anodes enabled by an in-situ generated mixed-ion/electron-conducting interface, Chem. Eng. J. 446 (2022) 136917, https://doi.org/10.1016/j.cej.2022.136917.

[39] Y. Li, Y.S. Hu, M.M. Titirici, L. Chen, X. Huang, Hard carbon microtubes made from renewable cotton as high-performance anode material for sodium-ion batteries, Adv. Energy Mater. 6 (2016) 1600659, https://doi.org/10.1002/aenm.201600659.

[40] M. Olson, J. Wheaton, M. Okkema, N. Oldham, S.W. Martin, Optimized thin film processing of sodium mixed oxy-sulfide-nitride glassy solid electrolytes for all-solid-state batteries, ACS Appl. Energy Mater. 6 (2023) 5842–5855, https://doi.org/10.1021/acsaem.3c00294.

[41] Y. Zhang, Z. Huang, H. Liu, H. Chen, Y. Wang, K. Wu, G. Wang, C. Wu, Amorphous phosphatized hybrid interfacial layer for dendrite-free sodium deposition, J. Power Sources 569 (2023) 233023, https://doi.org/10.1016/j.jpowsour.2023.233023.

[42] Y. Ouyang, Y. Guo, D. Li, Y. Wei, T. Zhai, H. Li, Single additive with dual functional-ions for stabilizing lithium anodes, ACS Appl. Mater. Interfaces 11 (2019) 11360–11368, https://doi.org/10.1021/acsami.8b21420.

[43] M. Wan, S. Kang, L. Wang, H.W. Lee, G.W. Zheng, Y. Cui, Y. Sun, Mechanical rolling formation of interpenetrated lithium metal/lithium tin alloy foil for ultrahigh-rate battery anode, Nat. Commun. 11 (2020) 829, https://doi.org/10.1038/s41467-020-14550-3.

[44] H. Wang, D. Lin, Y. Liu, Y. Li, Y. Cui, Ultrahigh-current density anodes with interconnected Li metal reservoir through overlithiation of mesoporous AlF_3 framework, Sci. Adv. 3 (2017) e1701301.

[45] X. Zheng, H. Fu, C. Hu, H. Xu, Y. Huang, J. Wen, H. Sun, W. Luo, Y. Huang, Toward a stable sodium metal anode in carbonate electrolyte: a compact, inorganic alloy interface, J. Phys. Chem. Lett. 10 (2019) 707–714, https://doi.org/10.1021/acs.jpclett.8b03536.

[46] X. Liang, Q. Pang, I.R. Kochetkov, M.S. Sempere, H. Huang, X. Sun, L.F. Nazar, A facile surface chemistry route to a stabilized lithium metal anode, Nat. Energy 2 (2017) 17119, https://doi.org/10.1038/nenergy.2017.119.

[47] Z. Zhu, L. Lu, Y. Yin, J. Shao, B. Shen, H. Yao, High rate and stable solid-state lithium metal batteries enabled by electronic and ionic mixed conducting network interlayers, ACS Appl. Mater. Interfaces 11 (2019) 16578–16585, https://doi.org/10.1021/acsami.9b02184.

[48] X. Fu, H. Duan, L. Zhang, Y. Hu, Y. Deng, A 3D framework with an in situ generated Li_3N solid electrolyte interphase for surerior lithium metal batteries, Adv. Funct. Mater. 33 (2023) 2308022, https://doi.org/10.1002/adfm.202308022.

[49] J. Sang, X. Zhang, K. Liu, G. Cao, R. Guo, S. Zhang, Z. Wu, Y. Zhang, R. Hou, Y. Shen, G. Shao, Effective coupling of amorphous selenium phosphide with high-conductivity graphene as resilient high-capacity anode for sodium-ion batteries, Adv. Funct. Mater. 33 (2023) 2211640, https://doi.org/10.1002/adfm.202211640.

[50] X. Liu, B. Xiao, A. Daali, X. Zhou, Z. Yu, X. Li, Y. Liu, L. Yin, Z. Yang, C. Zhao, L. Zhu, Y. Ren, L. Cheng, S. Ahmed, Z. Chen, X. Li, G. Xu, K. Amine, Stress and interface-compatible red phosphorus anode for high-energy and durable sodium-ion batteries, ACS Energy Lett. 6 (2021) 547–556, https://doi.org/10.1021/acsenergylett.0c02650.

[51] X. Zhou, F. Liu, Y. Wang, Y. Yao, Y. Shao, X. Rui, F. Wu, Y. Yu, Heterogeneous interfacial layers derived from the in situ reaction of CoF_2 nanoparticles with sodium metal for dendrite-free Na metal anodes, Adv. Energy Mater. 12 (2022) 2202323, https://doi.org/10.1002/aenm.202202323.

[52] I. Moeez, H.D. Lim, J.H. Park, H.G. Jung, K.Y. Chung, Electrochemically induced metallization of NaCl: use of the main component of salt as a cost-effective electrode material for sodium-ion batteries, ACS Energy Lett. 4 (2019) 2060–2068, https://doi.org/10.1021/acsenergylett.9b01118.

[53] K.J. Gaskell, P.M.A. Sherwood, Sodium phosphate dodecahydrate ($Na_3PO_4 \cdot 12H_2O$) by XPS, Surf. Sci. Spectra 9 (2002) 75–82, https://doi.org/10.1116/11.20030103.

[54] Thermo scientific avantage data system for XPS [Online], 2024. https://www.thermofisher.cn/cn/zh/home/materials-science/learning-center/periodic-table.html. (Accessed 2024-01-01 2024).

[55] L. Zhang, Y. Liu, J. Han, C. Yang, X. Zhou, Y. Yuan, Y. You, Al doped into Si/P sites of $Na_3Zr_2Si_2PO_{12}$ with conducted Na_3PO_4 impurities for enhanced ionic conductivity, ACS Appl. Mater. 15 (2023) 44867–44875, https://doi.org/10.1021/acsami.3c07680.

[56] M. Xu, Y. Li, M. Ihsan-Ul-Haq, N. Mubarak, Z. Liu, J. Wu, Z. Luo, J.K. Kim, NaF-rich solid electrolyte interphase for dendrite-free sodium metal batteries, Energy Stor. Mater. 44 (2022) 477–486, https://doi.org/10.1016/j.ensm.2021.10.038.

[57] J. He, A. Bhargav, L. Su, J. Lamb, J. Okasinski, W. Shin, A. Manthiram, Tuning the solvation structure with salts for stable sodium-metal batteries, Nat. Energy 9 (2024) 446–456, https://doi.org/10.1038/s41560-024-01469-y.

[58] B.D. Adams, J. Zheng, X. Ren, W. Xu, J.-G. Zhang, Accurate determination of coulombic efficiency for lithium metal anodes and lithium metal batteries, Adv. Energy Mater. 8 (2018) 1702097, https://doi.org/10.1002/aenm.201702097.

[59] F. Sun, R. Gao, D. Zhou, M. Osenberg, K. Dong, N. Kardjilov, A. Hilger, H. Markötter, P.M. Bieker, X. Liu, I. Manke, Revealing hidden facts of Li anode in cycled lithium-oxygen batteries through X-ray and neutron tomography, ACS Energy Lett. 4 (2019) 306–316, https://doi.org/10.1021/acsenergylett.8b02242.

[60] X. Zhang, S. Zhang, J. Lu, F. Tang, K. Dong, Z. Yu, A. Hilger, M. Osenberg, H. Markötter, F. Wilde, S. Zhang, J. Zhao, G. Xu, I. Manke, F. Sun, G. Cui, Unveiling the electro-chemo-mechanical failure mechanism of sodium metal anodes in sodium-oxygen batteries by synchrotron X-Ray computed tomography, Adv. Funct. Mater. 34 (2024) 2402253, https://doi.org/10.1002/adfm.202402253.

[61] J. Lu, S. Zhang, J. Yao, Z. Guo, M. Osenberg, A. Hilger, H. Markötter, F. Wilde, I. Manke, X. Zhang, F. Sun, G. Cui, Synergistic effect of CO_2 in accelerating the galvanic corrosion of lithium/sodium anodes in alkali metal-carbon dioxide batteries, ACS Nano 18 (2024) 10930–10945, https://doi.org/10.1021/acsnano.4c02329.

[62] L. Mo, A.-L. Chen, Y. Ouyang, W. Zong, Y.-E. Miao, T. Liu, Asymmetric sodiophilic host based on a Ag-modified carbon fiber framework for dendrite-free sodium metal anodes, ACS Appl. Mater. 13 (2021) 48634–48642, https://doi.org/10.1021/acsami.1c13018.

[63] Y. Wang, H. Dong, N. Katyal, H. Hao, P. Liu, H. Celio, G. Henkelman, J. Watt, D. Mitlin, A sodium-antimony-telluride intermetallic allows sodium-mental cycling at 100% depth of discharge and as an anode-free metal battery, Adv. Mater. 34 (2021) 2106005, https://doi.org/10.1002/adma.202106005.